Rotor Performance and Wake Interaction of Controlled Dual Surging FOWT Rotors in Tandem

Li, Yuan Tso; Yu, Wei; Sarlak, Hamid

DOI
10.1088/1742-6596/2767/9/092041

Publication date
2024

Document Version
Final published version

Published in
Journal of Physics: Conference Series

Citation (APA)
Li, Y. T., Yu, W., & Sarlak, H. (2024). Rotor Performance and Wake Interaction of Controlled Dual Surging FOWT Rotors in Tandem. *Journal of Physics: Conference Series*, *2767*(9), Article 092041. https://doi.org/10.1088/1742-6596/2767/9/092041

Rotor Performance and Wake Interaction of Controlled Dual Surging FOWT Rotors in Tandem

Journal of Physics: Conference Series **2767** (2024) 092041 doi:10.1088/1742-6596/2767/9/092041

Rotor Performance and Wake Interaction of Controlled Dual Surging FOWT Rotors in Tandem

YuanTso Li[1,2], Wei Yu[2], and Hamid Sarlak[1]

[1] Department of Wind and Energy Systems, Technical University of Denmark, DK-4000 Roskilde, Denmark

[2] Faculty of Aerospace Engineering, Delft University of Technology, Delft, The Netherlands

E-mail: hsar@dtu.dk

Abstract. Using Large Eddy Simulation (LES) with Actuator Line Model (ALM), this work investigates the system of two surging wind turbine rotors operating under realistic turbulent inflow conditions (TI = 5.3%). The two rotors are placed in tandem with a spacing of $5D$ and the surging motions are harmonic. A widely used torque controlling strategy, MPPT (Maximum Power Point Tracking), is implemented to ensure a maximium power extraction under all conditions. The rotor performances as well as the field data are surveyed to examine the effectiveness and impacts of the controller. It is found that the power performances of the surging rotors are benefited by the controller with a small margin ($\sim$ 1%) when the surging motions are moderate. The results also show that the controller reacts much slower than the considered surging frequency, making the power performances of the rotors worse than the quasi-steady predictions (targeted values) and complicating the system dynamics. In general, the implementation of the controller has minor impacts on the wake characteristics; however, the strengths of Surging Induced Periodic Coherent Structures (SIPCS) are found to be enhanced.

1. Introduction and Objectives

The concept of Floating Offshore Wind Farms (FOWFs) consisting of Floating Offshore Wind Turbines (FOWTs) has emerged in recent decades because it has an economical advantage over traditional bottom-fixed counterparts when the water depth is deeper than a certain limit ($\sim$ 60 m). Although the concept FOWF has become a promising means to unlock harvesting wind energy for sites with deeper water depths, several important aspects, such as the aerodynamics of wake interactions between FOWTs subject to motion, have not yet been thoroughly explored [1, 2]. Currently, only very few numerical studies in the literature have investigated wake interactions between FOWTs, and most of them either used models having lower fidelity or/and did not employ controlling strategies [3]. In light of this, this work simulated dual FOWT rotors in tandem using high-fidelity CFD models, namely Large Eddy Simulation (LES) with an Actuator Line Model (ALM), and a simple torque controller (MPPT, Maximum Power Point Tracking) is implemented. The tested simulations covered the cases with different surging configurations and with or without the controller equipped. The inter-spacing between the two rotors is chosen to be five rotor diameters ($5D$). The inflow conditions are set to be turbulent with a turbulence intensity of 5.3%, which is considered to be typical for offshore environments [4]. The main focus is to investigate how the implemented controller affected the

dual-rotor system with different surging configurations, where the rotor performances and two dimensional contour plots are investigated.

2. Methodology

2.1. Numerical setups

The full scale wind turbine rotor of NREL 5MW baseline turbine [5] is used, where its rotor diameter D is 126 m, rated wind speed $V_{0,\text{rated}}$ is 11.4 m/s, and rated rotor rotational speed Ω_{rated} is 1.27 rad/s. For simplicity, tower, tilt angles, pre-coning, floor effects, wind shear, and blade-aeroelastic are not considered. Furthermore, dynamic stall is not modeled with additional models since the chord based reduced frequencies k_c are rather low with the range of surging frequencies considered in this work ($k_c \leq 0.03$ for $r/R \geq 0.5$). For all simulation cases, the mean inflow wind speed V_0 is set to $V_{0,\text{rated}}$ and the two rotors are aligned in streamwise direction with a spacing of $5D$. The rotational speeds Ω are decided by the controller described in Section 2.3, or prescribed as Ω_{rated} and $2\Omega_{\text{rated}}/3$ for the upstream and downstream rotor of the uncontrolled cases, respectively. Also, for convenience, all power and thrust coefficients (C_P and C_T in Equation 1, where R is the rotor radius) are calculated based on $V_{0,\text{rated}}$ for both the upstream and downstream rotor.

$$C_P = \frac{P}{0.5\rho V_{0,\text{rated}}^3 \pi R^2}, \qquad C_T = \frac{T}{0.5\rho V_{0,\text{rated}}^2 \pi R^2} \tag{1}$$

Simulations are carried out with *OpenFOAM v2106*. The standard Smagorinsky model is selected and the mesh consists of 10.9M cubic cells with the computational domain being $16D \times 5D \times 5D$. Turbulent inflow conditions are realized with a OpenFOAM's built-in synthetic turbulent inlet conditions DFSEM (divergence-free synthetic eddy method) [6]. ALM is implemented with modules of *turbinesFoam* developed by Bachant *et al.* [7]. Each blade is represented with 40 actuator line points with equidistant, and the gird resolution of the rotors and wakes is set to $D/80$. The time step size Δt is set to fulfill $\Omega_{\text{rated}}\Delta t = 1^\circ$, ensuring that the blade-tip travels less than one gird size per time step. PISO (Pressure-Implicit with Splitting of Operators) algorithm is implemented to solve the coupled pressure-velocity system of equations system. The duration of statistics is $50T_{\Omega,\text{rated}}$ ($T_{\Omega,\text{rated}}$ is the rotor rotational period for a NREL 5MW rotor at its rated conditions), and solutions of the initial stages are disregarded to avoid transient effects. See Li [8] for validation, verification, more detailed documentation.

2.2. Surging settings and phase-locking averaging

The positions of the surging FOWT rotors, denoted as p_R^{up} and p_R^{down}, are described by Equations 2 and 3 (superscripts up and down indicate that the parameter is for the upstream or downstream rotor). Here, $p_{R_0}^{\text{up}}$ and $p_{R_0}^{\text{down}}$ represent the neutral positions of the rotors, A_S and ω_S stand for the surging amplitude and frequency, and ϕ_S is the phase angle of the surging motions (the initial phase shifts are set to 0.0π for all rotors). Surging settings for the upstream and downstream rotor within a case are set to be identical, considering the motions are mainly affected by hydrodynamic loads [9]. With the surging motions defined, the surging velocity of the rotor V_S can be calculated, as shown on the left side of Equation 4. As the rotor is subjected to surging motion, the apparent inflow velocity seen by the rotor, denoted as $V_{0,\text{app}}$, is affected by V_S, as given on the right-hand side of Equation 4. Note that $V_{0,\text{app}}$ increases with negative V_S according to the coordinate system used.

$$p_R^{\text{up}}(t) = A_S^{\text{up}} \sin\left(\omega_S^{\text{up}} t\right) + p_{R_0}^{\text{up}} = A_S^{\text{up}} \sin\phi_S^{\text{up}} + p_{R_0}^{\text{up}} \tag{2}$$

$$p_R^{\text{down}}(t) = A_S^{\text{down}} \sin\left(\omega_S^{\text{down}} t\right) + p_{R_0}^{\text{down}} = A_S^{\text{down}} \sin\phi_S^{\text{down}} + p_{R_0}^{\text{down}} \tag{3}$$

$$V_S = \frac{\mathrm{d}p_R(t)}{\mathrm{d}t} = A_S\omega_S\cos(\phi_S), \qquad V_{0,\mathrm{app}} = V_0 - V_S \tag{4}$$

For FOWT rotors subjected to harmonic surging motions, there are two important non-dimensional parameters, which are the ratio of the maximum surging velocity to the freestream velocity, denoted as $\mathcal{V}$, and the reduced frequency based on the rotor diameter, denoted as $\mathcal{W}$, respectively. Their definitions are given in Equation 5. To provide an example, when applying a surging motion with $A_S = 4$ m and $\omega_S = 0.63$ rad/s to a NREL 5MW rotor under its rated conditions, $\mathcal{V}$ and $\mathcal{W}$ will be 0.22 and 7.0, respectively. Note that $\mathcal{V}$ and $\mathcal{W}$ can be understood as the *magnitude of surging* and the *rate of surging* [10].

$$\mathcal{V} \triangleq \frac{V_{S,\max}}{V_0} = \frac{A_S\omega_S}{V_0}, \qquad \mathcal{W} \triangleq \frac{\omega_S D}{V_0} \tag{5}$$

To better understand the impacts of surging motions, some of the analyses are based on the quantities sampled at a rate of ω_S. That is, data are sampled at a certain ϕ_S. Taking u as an example, these data are denoted as u_{ϕ_S}, and they are called *phase-locking* data. The average based on these data are called *phase-locking averaged* data, which is denoted as $< u >_{\phi_S}$. Equation 6 gives the relation between u_{ϕ_S} and $< u >_{\phi_S}$ by letting $\phi_S = 0.0\pi$, where N is the number of samples of phase-locking data. If the phase-locking averaging is conducted over an entire surging cycle, we called it *cycle-averaged* data. See Figure 1(b) for an example of cycle-averaged C_P, which is denoted as $< C_P >$.

$$< u >_{0\pi} = \frac{\sum_{n=1}^{N} u_{0\pi,n}}{N} \tag{6}$$

2.3. Optimal torque (MPPT) controller

The controller implemented in this paper involves only adjustment of rotor speed Ω (variable speed, constant pitch angle), which is the torque controller commonly used to realize Maximum Power Point Tracking (MPPT) [11, 12], and the working principle is to make the rotor operate with a certain tip speed ratio λ_{opt} that gives the optimal (desired) C_P ($C_{P,\mathrm{opt}}$). In real-world, the controller works by actively adjusting the generator torque τ_{Gen} according to Ω, as briefly described from Equation 7 to 9, where P_{Gen} and P_{Aero} are the generator and aerodynamic power, τ_{Gen} and τ_{Aero} are the generator and aerodynamic torque, $P_{\mathrm{Aero,opt}}$ is the optimal aerodynamic power of the rotor, and V is the instantaneous inflow velocity seen by the rotor.

$$P_{\mathrm{Aero,opt}} = \frac{1}{2}\rho\pi R^2 V^3 C_{P,\mathrm{opt}} = \frac{\rho\pi R^5 C_{P,\mathrm{opt}}}{2\lambda_{\mathrm{opt}}^3}\Omega^3, \qquad P_{\mathrm{Gen}} = \tau_{\mathrm{Gen}}\Omega \tag{7}$$

$$\text{for} \quad P_{\mathrm{Gen}} = P_{\mathrm{Aero,opt}} \quad \rightarrow \quad \tau_{\mathrm{Gen}} = \frac{\rho\pi R^5 C_{P,\mathrm{opt}}}{2\lambda_{\mathrm{opt}}^3}\Omega^2 \tag{8}$$

$$I\frac{\mathrm{d}\Omega}{\mathrm{d}t} = \frac{P_{\mathrm{Aero}}}{\Omega} - \tau_{\mathrm{Gen}} = \tau_{\mathrm{Aero}} - \tau_{\mathrm{Gen}} \triangleq \Delta\tau, \qquad \Omega(t+\Delta t) \simeq \Omega(t) + \frac{\mathrm{d}\Omega}{\mathrm{d}t}\Delta t \tag{9}$$

$$\Omega_{\mathrm{Tar}} = \frac{\lambda_{\mathrm{opt}} V_{0,\mathrm{app}}}{R}, \qquad C_{P,\mathrm{Tar}} = C_{P,\mathrm{opt}}\left(\frac{V_{0,\mathrm{app}}}{V_{0,\mathrm{rated}}}\right)^3 \tag{10}$$

The main goal is to match P_{Gen} with $P_{\mathrm{Aero,opt}}$ by making $P_{\mathrm{Aero}} = P_{\mathrm{Aero,opt}}$, so that the electric power converted by the generator equals the optimal aerodynamic power of the rotor ($P_{\mathrm{Gen}} = P_{\mathrm{Aero,opt}}$). One of the main advantages of this controller is that it only needs the measurement of Ω, which is rather easy to obtain for a wind turbine in real-world. However, its

major drawback is that its reaction time is rather long, and this is going to be displayed later with our results. See Manwell *et al.* [11] and Abbas *et al.* [12] for more detailed descriptions about the controller. For convenience, we approximate the optimal C_P and λ with the rated ones, that is, making $C_{P,\text{opt}} = C_{P,\text{rated}} = 0.5177$ and $\lambda_{\text{opt}} = \lambda_{\text{rated}} = 7.00$. $C_{P,\text{rated}}$ is based on the value of $\overline{C}_{P,\text{Gen}}$ for case **1** in Table 1. Also, since there are P_{Aero} and P_{Gen}, there are two C_P, namely $C_{P,\text{Aero}}$ and $C_{P,\text{Gen}}$ for the controlled cases. Note that for the analysis of power outputs in this work, quantities of generator are used if not mentioned otherwise. Moreover, we introduce targeted Ω and C_P, denoted as Ω_{Tar} and $C_{P,\text{Tar}}$, as described in Equation 10. These are the targeted values of Ω and C_P for the controlled cases based on the quasi-steady predictions using $V_{0,\text{app}}$. See Li [8] for more detailed documentation.

3. Test metrics and basic results

The setups for the simulation cases are listed in Table 1, and to avoid repetition, the representative results such as $\overline{C}_P$ and $\overline{C}_T$ are concatenated. The subscripts *Gen*, *Aero*, and *Tar* stand for *generator*, *aerodynamic* and *targeted*. The superscripts indicate the parameter is for upstream or downstream rotor, and the overline stands for time averaging (all available time steps are considered). Note that $C_{P,\text{Gen}}$ and $C_{P,\text{Aero}}$ for the uncontrolled cases are equivalent.

Based on the analysis of the previous studies [13, 14], for typical sea states, the selected surging parameters include the typical surging response of the floating platforms ($A_S \simeq 2$ m and $\omega_S \simeq 0.63$ rad/s, i.e. $\mathcal{V} \simeq 0.11$ and $\mathcal{W} \simeq 7.0$, assuming being tension leg platform) and fall within the realistic range.

Table 1. Case settings and results for the simulations conducted with dual FOWT rotors with a spacing of $5D$. "O" indicates the MPPT controller is implemented while "X" indicates the opposite. Subscripts Gen, Aero, and Tar indicate the values are for generator, aerodynamic, or targeted values (Equation 10). Surging settings are characterized by $\mathcal{V}$ and $\mathcal{W}$ (Equation 5).

Case	Con.	$\mathcal{V}$	$\mathcal{W}$	Inertia	$\overline{C}_T^{\text{up}}$	$\overline{C}_{P,\text{Gen}}^{\text{up}}$	$\overline{C}_{P,\text{Aero}}^{\text{up}}$	$\overline{C}_{P,\text{Tar}}^{\text{up}}$	$\overline{C}_T^{\text{down}}$	$\overline{C}_{P,\text{Gen}}^{\text{down}}$	$\overline{C}_{P,\text{Aero}}^{\text{down}}$	$\sum \overline{C}_{P,\text{Gen}}$
1	X	**0.00**	–	–	**0.726**	**0.518**	–	–	**0.344**	**0.181**	–	**0.699**
2	X	0.11	7.0	–	0.725	0.522	–	–	0.343	0.183	–	0.705
3	X	0.22	7.0	–	0.716	0.525	–	–	0.332	0.178	–	0.703
4	X	0.44	7.0	–	0.673	0.516	–	–	0.301	0.160	–	0.676
C1	**O**	**0.00**	–	**Regular**	**0.726**	**0.518**	**0.518**	**0.518**	**0.379**	**0.199**	**0.199**	**0.716**
C2	O	0.11	7.0	Regular	0.728	0.524	0.523	0.527	0.379	0.201	0.202	0.725
C3	O	0.22	7.0	Regular	0.721	0.531	0.531	0.556	0.369	0.201	0.201	0.732
C4	O	0.44	7.0	Regular	0.665	0.513	0.512	0.671	0.307	0.167	0.167	0.679
C5	O	0.22	7.0	Smaller	0.754	0.583	0.583	0.556	0.370	0.218	0.218	0.800
C6	O	0.11	3.5	Regular	0.729	0.525	0.525	0.527	0.376	0.198	0.198	0.723

4. Rotor rotational speed and power outputs with different surging amplitudes

Figures 1 and 2 show the cycle-averaged Ω and C_P ($< \Omega >$ and $< C_P >$) of the upstream and downstream rotor for cases **C1**-**C4** (the cycle-averaged quantities for the fixed case are based on a frequency of 0.63 rad/s). The focus of this subsection is on inspecting the performances of both the upstream and downstream rotors for the controlled cases with different $\mathcal{V}$ but same $\mathcal{W}$ (different A_S, same ω_S).

Cycle-averaged properties for the upstream rotor The analysis begins by examining $< \Omega^{\text{up}} >$ in Figure 1(a). For the fixed case (case **C1**), $< \Omega_{\text{Gen}}^{\text{up}} >$ remains constant and matches Ω_{rated}, which is as designed. In contrast, the surging cases (cases **C2**-**C4**) exhibit increasing fluctuations in $< \Omega_{\text{Gen}}^{\text{up}} >$ with larger $\mathcal{V}$ and their $< \Omega_{\text{Gen}}^{\text{up}} >$ significantly deviate from $< \Omega_{\text{Tar}}^{\text{up}} >$. $< \Omega_{\text{Gen}}^{\text{up}} >$ for

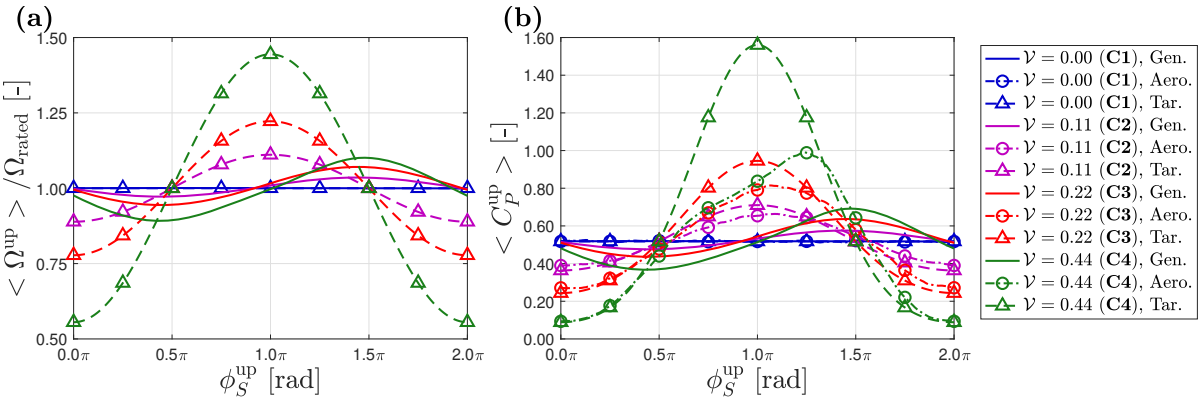

Figure 1. Cycle-averaged Ω^{up} and C_P^{up} for the controlled cases in Table 1. Numbers in the parentheses indicates the case number.

the surging cases lag behind their $< \Omega^{\mathrm{up}}_{\mathrm{Tar}} >$ and have smaller fluctuations compared to those of $< \Omega^{\mathrm{up}}_{\mathrm{Tar}} >$. The reasons behind will be elucidated together with the analysis of $< C_P^{\mathrm{up}} >$ later.

The analysis progresses with $< C_P^{\mathrm{up}} >$ using $< C^{\mathrm{up}}_{\mathrm{P,Gen}} >$, $< C^{\mathrm{up}}_{\mathrm{P,Aero}} >$, and $< C^{\mathrm{up}}_{\mathrm{P,Tar}} >$ plotted in Figure 1(b). It is observed that $< C^{\mathrm{up}}_{\mathrm{P,Gen}} >$ lags significantly behind $< C^{\mathrm{up}}_{\mathrm{P,Tar}} >$ as $< \Omega^{\mathrm{up}}_{\mathrm{Gen}} >$ and $< \Omega^{\mathrm{up}}_{\mathrm{Tar}} >$ observed earlier. Meanwhile, $< C^{\mathrm{up}}_{\mathrm{P,Aero}} >$ lags slightly behind $< C^{\mathrm{up}}_{\mathrm{P,Tar}} >$ (but leads $< C^{\mathrm{up}}_{\mathrm{P,Gen}} >$). The lag of $< C^{\mathrm{up}}_{P,\mathrm{Gen}} >$ is attributed to its sole dependence on $< \Omega^{\mathrm{up}}_{\mathrm{Gen}} >$ (Equations 7 and 8), which responds to $< C^{\mathrm{up}}_{P,\mathrm{Aero}} >$ through $\Delta\tau$, as shown in Equation 9. $< C^{\mathrm{up}}_{P,\mathrm{Aero}} >$ lags behind $< C^{\mathrm{up}}_{P,\mathrm{Tar}} >$ because it is partially influenced by $< \Omega^{\mathrm{up}}_{\mathrm{Gen}} >$, as changes in $< \Omega^{\mathrm{up}}_{\mathrm{Gen}} >$ impact the operational conditions of the rotor. Note that the actual driving force to adjust $< \Omega^{\mathrm{up}}_{\mathrm{Gen}} >$, $\Delta\tau$, can be evaluated through $< C^{\mathrm{up}}_{P,\mathrm{Aero}} >$ and $< C^{\mathrm{up}}_{P,\mathrm{Gen}} >$ presented in the figure. Clearly, the cases with larger $\mathcal{V}$ have larger values for $\Delta\tau$ and therefore have higher fluctuation amplitudes for $< \Omega^{\mathrm{up}}_{\mathrm{Gen}} >$, as shown in Figure 1(a). Additionally, the lag of $< \Omega^{\mathrm{up}}_{\mathrm{Gen}} >$ causes the fluctuation amplitudes of $< C^{\mathrm{up}}_{P,\mathrm{Gen}} >$ to be smaller than $< C^{\mathrm{up}}_{P,\mathrm{Aero}} >$, and both $< C^{\mathrm{up}}_{P,\mathrm{Gen}} >$ and $< C^{\mathrm{up}}_{P,\mathrm{Aero}} >$ have smaller fluctuations than $< C^{\mathrm{up}}_{P,\mathrm{Tar}} >$.

The analysis carried out so far suggests that the rotational inertia of the rotor (I) is high. This high inertia causes the FOWT system to respond slowly against the changing aerodynamic inputs, such as the varying $V_{0,\mathrm{app}}$, making the operational conditions of the system deviate from the designed (targeted) values. (I is 4.39×10^7 kg m^2 according to the documentation of Jonkman *et al.* [5].) Consequently, the fluctuation amplitudes of the cycle-averaged quantities measured (Gen and Aero) are all smaller than those of the quasi-steady predictions (Tar). Further investigation to confirm that large I is the cause of slow response is presented in Section 6, where a scenario with smaller I is examined. Furthermore, due to the lagging effects of the implemented controller, accurately estimating $V_{0,\mathrm{app}}$ of a real-world FOWT based solely on the measured Ω_{Gen} can be challenging if the same MPPT controller is used.

Cycle-averaged properties for the downstream rotor Figures 2(a) and 2(b) show the cycle-averaged quantities of the downstream rotor for cases **C1-C4**. Since predicting the inflow velocity seen by the downstream rotor is challenging due to the wake of the upstream rotor, $< \Omega^{\mathrm{down}}_{\mathrm{Tar}} >$ and $< C^{\mathrm{down}}_{P,\mathrm{Tar}} >$ are not provided. $< \Omega^{\mathrm{down}}_{\mathrm{Gen}} >$ for the fixed case (case **C1**) maintains a nearly constant value but differs from the prescribed values ($2\Omega_{\mathrm{rated}}/3$) for the cases without the controller implemented (cases **1-4**), indicating $< \Omega^{\mathrm{down}}_{\mathrm{Gen}} >$ for the controlled case is adjusted. In contrast, for the other three surging cases, $< \Omega^{\mathrm{down}}_{\mathrm{Gen}} >$ exhibits fluctuations in response to the surging motion. Interestingly, unlike $< \Omega^{\mathrm{up}}_{\mathrm{Gen}} >$, where the four cases share a similar mean

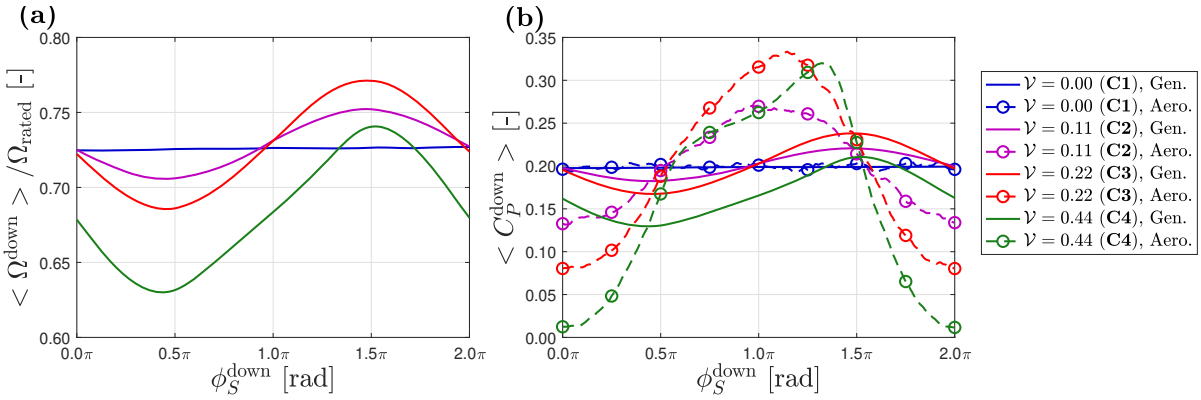

Figure 2. Cycle-averaged Ω^{down} and C_P^{down} for the controlled cases in Table 1.

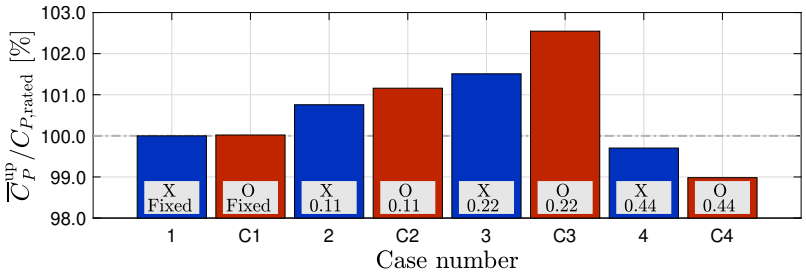

Figure 3. Bar graph of time-averaged $\overline{C}_P^{\text{up}}$ for the cases in Table 1. Entries for each bar stands for whether the cases are controlled ("O"/"X" for controlled/uncontrolled) and values of $\mathcal{V}$.

value, $< \Omega_{\text{Gen}}^{\text{down}} >$ of case **C4** with $\mathcal{V} = 0.44$ has a different mean value compared to the other. This difference in mean of $\Omega_{\text{Gen}}^{\text{down}}$ for case **C4** can be attributed to severe stalling experienced by the surging downstream rotor. Under identical surging conditions, stalling due to surging motions is more pronounced for the downstream rotor due to its larger effective $\mathcal{V}$ compared to the upstream one, since the effective V_0 experienced by the downstream rotor is reduced by wake effects (see Li [8] for more details). Moreover, this shift in mean values underscores the complex dynamics due to the interplay of surging motions, rotor aerodynamics, wake interactions, and the controller. As to $< C_P^{\text{down}} >$, it is evident once again that $< C_{P,\text{Gen}}^{\text{down}} >$ lags behind $< C_{P,\text{Aero}}^{\text{down}} >$, with $< C_{P,\text{Aero}}^{\text{down}} >$ displaying larger fluctuation amplitudes. This is again due to the large I of the system.

5. Compare cases with and without controller

To analyze the effectiveness of the controller, we compare the results of the cases with the controller implemented (cases **C1**-**C4**) to the cases without (cases **1**-**4**). Both rotor performance and wake characteristics are evaluated. Note that the analysis of rotor performance in this section focuses only on the upstream rotor, since the downstream rotor is influenced by too many variables, making the system too complex for focused analysis.

Time-averaged power performance To provide a clearer visual representation of the results, time-averaged power coefficient for the eight cases list in Table 1 are presented with a bar graph in Figure 3. $\overline{C}_{P,\text{Gen}}^{\text{up}}$ for the two fixed cases in Figure 3 perfectly match $C_{P,\text{rated}}$, meeting the expectation (the controller is designed based on $C_{P,\text{rated}}$, which is $\overline{C}_{P,\text{Gen}}^{\text{up}}$ for case **1**). $\overline{C}_{P,\text{Gen}}^{\text{up}}$ of the surging cases without the controller implemented follow what Li *et al.* [10] reported. The

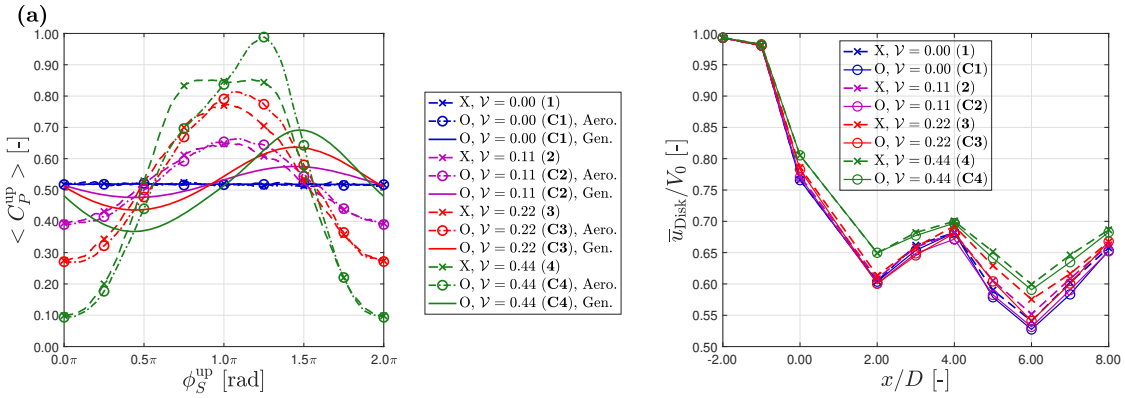

Figure 4. Cycle-averaged C_P^{up} (a) and $\overline{u}_{\mathrm{Disk}}$ (b) for the controlled and uncontrolled cases.

values of $\overline{C}_{P,\mathrm{Gen}}^{\mathrm{up}}$ are improved when subjected to moderate surging motions (cases with $\mathcal{V} \leq 0.22$ in Table 1), but these values are reduced when the cases experience severe stalling (cases with $\mathcal{V} \geq 0.44$). Our current results show that the implementation of the controller further improves the already increased $\overline{C}_{P,\mathrm{Gen}}^{\mathrm{up}}$ by around 1% the for cases with $\mathcal{V} \leq 0.22$. For a controlled surging rotor, gains in $\overline{C}_{P,\mathrm{Gen}}^{\mathrm{up}}$ compared to a fixed rotor reach around 2.5%, similar to what Johlas *et al.* [15] reported, in which they simulated the FOWT subjected to typical sea states using LES coupled with hydro-servo-aero-elastic solver. However, it is clear that $\overline{C}_{P,\mathrm{Gen}}^{\mathrm{up}}$ obtained for the controlled cases remain significantly lower than $\overline{C}_{P,\mathrm{Tar}}^{\mathrm{up}}$ as can be seen in Table 1, indicating the power performance of the surging rotor is well below its maximum potential. This is primarily attributed to the substantial rotational inertia of the rotor that delays the system response. In the case that experienced severe stalling (case **C4**), our results indicate that the implementation of the controller leads to a further decrease in $\overline{C}_{P,\mathrm{Gen}}^{\mathrm{up}}$, illustrating the limitations of the current controlling strategy as well as the complex aerodynamics of the controlled surging FOWT rotor.

Cycle-averaged power performance Figure 4(a) displays $< C_P^{\mathrm{up}} >$ of the eight cases. It shows that the fluctuation amplitudes of $< C_{P,\mathrm{Aero}}^{\mathrm{up}} >$ for the controlled cases are larger than those of $< C_P^{\mathrm{up}} >$ for the uncontrolled cases, while $< C_{P,\mathrm{Gen}}^{\mathrm{up}} >$ for the controlled cases have further smaller ranges. These indicate that the controller effectively adjusts the aerodynamic performance of the rotor during a surging cycle, while the large inertia of the system confines the fluctuation of the output generator power. Furthermore, $< C_{P,\mathrm{Aero}}^{\mathrm{up}} >$ for the controlled cases with a surging rotor no longer has symmetry about $\phi_S = 1.0\pi$ as $< C_P^{\mathrm{up}} >$ for the cases without controller does, and this is directly related to the phase delay of $< \Omega_{\mathrm{Gen}}^{\mathrm{up}} >$ described earlier.

Wake characteristics and wake structures The mean area-averaged streamwise velocity (area within the rotor radius), denoted as $\overline{u}_{\mathrm{Disk}}$, along the x-direction for the eight cases are presented in Figure 4(b). It can be seen that $\overline{u}_{\mathrm{Disk}}$ for the cases with surging rotors is higher compare to the cases with fixed rotors, as reported by Li *et al.* [10]. Moreover, comparing the cases with and without the controller at the same $\mathcal{V}$ reveals that the implementation of the controller has limited impacts on $\overline{u}_{\mathrm{Disk}}$. In general, the uncontrolled cases tend to have slightly higher values of $\overline{u}_{\mathrm{Disk}}$. This can be attributed to the fact that the controlled cases extracted more energy from the flow, as they have higher $\overline{C}_{P,\mathrm{Gen}}$.

In terms of analysis about the wake structures, only the four most representative scenario are displayed, which are uncontrolled-fixed (case **1**), uncontrolled-surging (case **3**), controlled-fixed (case **C1**), and controlled-surging (case **C3**). The instantaneous streamwise velocity (u) fields

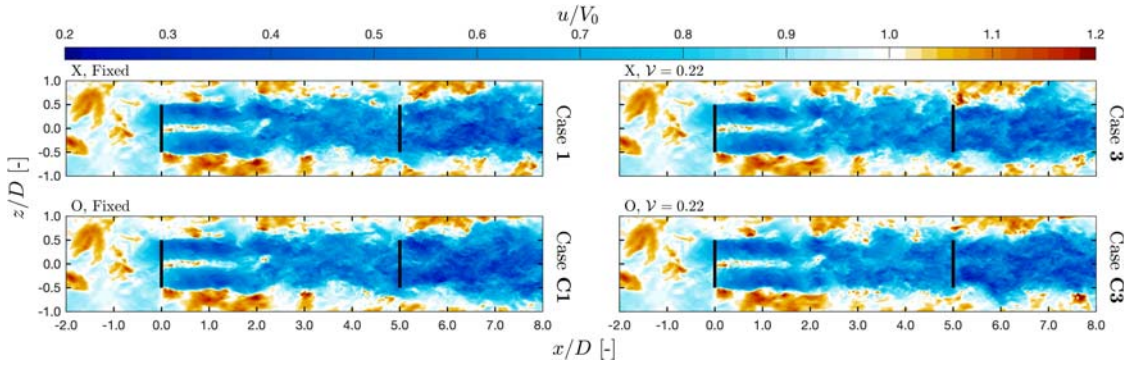

Figure 5. Contours of u (instantaneous streamwise velocity). Black lines indicate the rotors. Whether the cases are controlled and values of $\mathcal{V}$ are indicated at top-left for each panel.

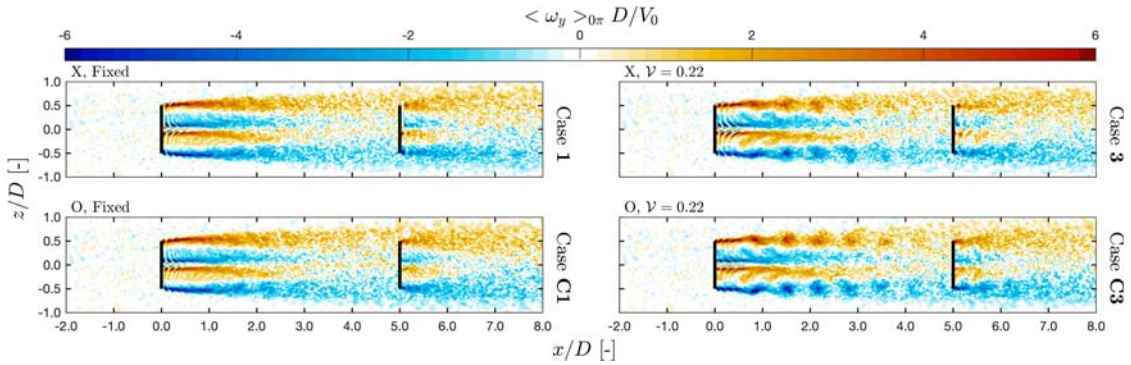

Figure 6. Contours of $< \omega_y >_{0\pi}$ (phase-locking averaged vorticity). Black lines indicate the rotors. Whether the cases are controlled and values of $\mathcal{V}$ are indicated at top-left for each panel.

of these four cases depicted in Figure 5 show that both the surging motions and the controller have limited impacts (almost unidentifiable by visual inspection), which is as expected based on the results reported by Li *et al.* [10]. As to the phase-locking averaged y-component (out-of-plane component) vorticity fields, denoted as $< \omega_y >_{0\pi}$, in Figure 6, noticeable differences are detected between the fixed and surging cases, where Surging Induced Periodic Coherent Structures (SIPCS, introduced in Li *et al.* [10]) are observed in the two surging cases. More interestingly, SIPCS for the controlled-surging case (case **C3**) have sharper contours than those of the uncontrolled-surging case (case **3**), showing that the strengths of SIPCS for the controlled-surging case are stronger and shows that the implementation of the controller magnified the periodicity of the system. This highlights that the controller may significantly affect the wake aerodynamics of FOWTs.

6. Impacts of the rotational inertia

The results in the previous sections show that the controller implemented in this work requires a relatively long timescale (compared to the interested surging periods) to fully respond, and the large rotational inertia I of the rotor system (rotor plus drive train) is suspected to be the cause. To test the hypothesis, an additional case is conducted with a smaller I, where its I is set to be 1/50 of the regular one. The test case is case **C5** in Table 1, and except for the values of I, all the other parameters for the test case are identical to those of case **C3**.

Figure 7(a) plots $< C_P^{\text{up}} >$ for the test case (smaller I) and the reference case (regular I). It can be seen that $< C_{P,\text{Aero}}^{\text{up}} >$ and $< C_{P,\text{Gen}}^{\text{up}} >$ for the case with a smaller I in Figure 7 almost

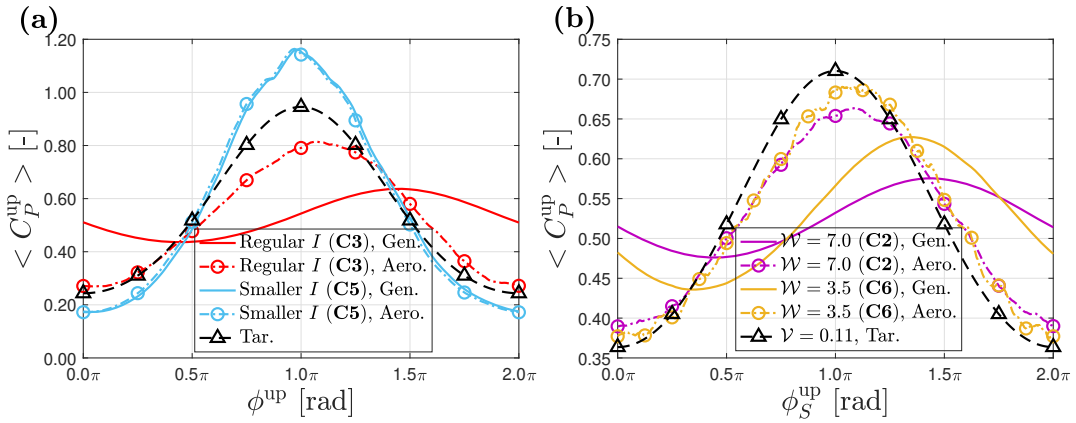

Figure 7. Comparing the cycle-averaged C_P^{up} for cases with different rotor rotational inertia I (a) and with different $\mathcal{W}$ (b). Numbers in the parentheses indicate the case number in Table 1.

follow the same curve, with $< C_{P,\mathrm{Gen}}^{\mathrm{up}} >$ lags only a little. This shows that the controller adjusts the rotational speed of the rotor ($< \Omega_{\mathrm{Gen}}^{\mathrm{up}} >$) almost immediately according to the aerodynamic input (the slight lag is inevitable due to the nature of Equation 9). Considering $< C_{P,\mathrm{Aero}}^{\mathrm{up}} >$, $< C_{P,\mathrm{Gen}}^{\mathrm{up}} >$, and $< C_{P,\mathrm{Tar}}^{\mathrm{up}} >$ for the test case (almost) share a same phase, it can be concluded that large I is the cause of the phase delay observed in the reference case.

As to the fluctuating amplitudes of the test case, $< C_{P,\mathrm{Gen}}^{\mathrm{up}} >$ for it is much larger than for the reference case. Furthermore, very interestingly, even though the curves of $< C_{P,\mathrm{Gen}}^{\mathrm{up}} >$ and $< C_{P,\mathrm{Tar}}^{\mathrm{up}} >$ show almost no phase differences, the two curves have significant discrepancies in their values, with $< C_{P,\mathrm{Gen}}^{\mathrm{up}} >$ ranging considerably wider than $< C_{P,\mathrm{Tar}}^{\mathrm{up}} >$. Moreover, the value for $\overline{C}_{P,\mathrm{Gen}}^{\mathrm{up}}$ is even higher than the value for $\overline{C}_{P,\mathrm{Tar}}^{\mathrm{up}}$. This suggests that hysteresis (unsteady aerodynamics) effects (specifically, induction lagging [16]) play a significant role in the test case here. Note that for the settings of harmonic surging ($\mathcal{V}$ and $\mathcal{W}$) considered in this current work, most previous studies (e.g., Li *et al.* [10]) show that the hysteresis effects are little when it comes to the rotor performance. However, most of those works neglect the controller completely, and the test case here is fundamentally different from them by altering the rotor rotational speed considerably. These results again highlight the complex aerodynamics of the controlled FOWT system, and a complete understanding of it is still lacking in the current literature.

7. Impacts of the surging frequency

Section 6 demonstrates that the slow response of the MPPT controller is attributed to the large I of the NREL 5MW rotor, making the values of $\overline{C}_{P,\mathrm{Gen}}^{\mathrm{up}}$ for cases **C2-C4** (controlled-surging cases) falling short of their quasi-steady predictions ($\overline{C}_{P,\mathrm{Tar}}^{\mathrm{up}}$). Therefore, there is a compelling interest in investigating the frequency response of the controller, understanding whether giving it more time to respond will bring the simulation results closer to the quasi-steady predictions. Motivated by this, we perform an additional case based on the setup of case **C3** but halving the surging frequency ω_S (equivalent in halving $\mathcal{W}$), which is case **C6** in Table 1. Note that since halving ω_S changes both $\mathcal{V}$ and $\mathcal{W}$ while $< C_{P,\mathrm{Tar}}^{\mathrm{up}} >$ is mainly dominated by $\mathcal{V}$, instead of case **C3**, case **C6** is compared to case **C2**, as both case **C2** and case **C6** have the same values for $\mathcal{V}$.

Figure 7(b) presents a comparison between the curves of $< C_P^{\mathrm{up}} >$ of the test case (with lower $\mathcal{W}$) and the reference case (with higher $\mathcal{W}$). These two cases share the same curve for $< C_{P,\mathrm{Tar}}^{\mathrm{up}} >$ as they have the same value for $\mathcal{V}$. Notably, both the phase and the fluctuating amplitude of $< C_{P,\mathrm{Gen}}^{\mathrm{up}} >$ for the test case are brought closer to those of $< C_{P,\mathrm{Tar}}^{\mathrm{up}} >$ compared

to the reference case, demonstrating that the current MPPT controller is more effective in the scenario with a lower surging frequency.

8. Conclusion

In this work, simulations with dual surging or fixed rotors of NREL 5MW baseline turbine had been conducted. Cases with or without the implementation of the simple torque controller (Maximum Power Point Tracking, MPPT), cases having different surging settings, and cases having different rotor rotational inertia are tested and compared. The major discoveries and conclusions are as follows. With the surging settings tested, the implemented controller was unable to adjust the operational conditions (rotational speed, Ω_{Gen}) of the surging rotor fast enough to meet the designed operational conditions. The main reason is that the rotational inertia of the rotor I is large, slowing down the adaptation of the rotational speed. Additionally, it is shown that the periodicity of surging rotor's wake structures was further strengthened with the implementation of the MPPT controller, confirming that the wake aerodynamics of FOWTs were affected by the controller.

In general, for the controlled-surging cases, the total power outputted was improved by the controller when subjected to moderate surging motions, while the implementation of the controller may cause losses if surging motions led to severe stalling. Moreover, these improvements due to the controller were only marginally ($\sim 1\%$) and are much lower than the targeted values (quasi-steady predictions). Furthermore, it is shown that with a lower surging frequency, the controller was able to adjust the rotational speed of the rotor more effectively. Additionally, our results also showed that if the rotational speed of the FOWT was quickly adjusted, the hysteresis (unsteady aerodynamics) effects would become significant.

The results presented in this study indicate that to make the power output of FOWT subjected to periodic motions closer to the quasi-steady prediction, more sophisticated control strategies may be required. Potential improvements could involve taking into account the rotor inertia, such as methods that consider the time derivative of Ω_{Gen} [17]. Furthermore, further research with more extensive setups, such as imposing different types of motion or equipping different controlling strategies, is recommended, as the controller may affect the aerodynamics, wake structures, and wake interactions of FOWTs in different manners when they are subjected to other types of motion other than surging, e.g., pitching and swaying.

References

[1] van Kuik G, Peinke J, Nijssen R, Lekou D, Mann J, Sørensen J N, Ferreira C, van Wingerden J W, Schlipf D, Gebraad P *et al.* 2016 *Wind energy science* **1** 1–39
[2] Veers P, Dykes K, Lantz E, Barth S, Bottasso C L, Carlson O, Clifton A, Green J, Green P, Holttinen H *et al.* 2019 *Science* **366** eaau2027
[3] Micallef D and Rezaeiha A 2021 *Renewable and Sustainable Energy Reviews* **152** 111696
[4] Hansen K S, Barthelmie R J, Jensen L E and Sommer A 2012 *Wind Energy* **15** 183–196
[5] Jonkman J, Butterfield S, Musial W and Scott G 2009 Tech. rep. NREL Golden, CO, US
[6] Poletto R, Craft T and Revell A 2013 *Flow, turbulence and combustion* **91** 519–539
[7] Pete Bachant, Anders Goude, Daa-mec, Martin Wosnik 2019 turbinesFoam: v0.1.1
[8] Li Y 2023 (Delft University of Technology, thesis)
[9] Cheng P, Huang Y and Wan D 2019 *Ocean Engineering* **173** 183–196
[10] Li Y, Yu W and Sarlak H 2023 *arXiv preprint arXiv:2310.08655*
[11] Manwell J F, McGowan J G and Rogers A L 2010 (John Wiley & Sons)
[12] Abbas N J, Wright A and Pao L 2020 *Journal of Physics: Conference Series* vol 1452 p 012002
[13] Kyle R, Lee Y C and Früh W G 2020 *Renewable Energy* **155** 645–657
[14] Wen B, Tian X, Dong X, Peng Z and Zhang W 2018 *Wind Energy* **21** 1076–1091
[15] Johlas H M, Martínez-Tossas L A, Churchfield M J, Lackner M A and Schmidt D P 2021 *Wind Energy* **24** 901–916
[16] Leishman J G 2002 *Wind Energy* **5** 85–132
[17] Zhang X, Jia J, Zheng L, Yi W and Zhang Z 2023 *Energy Science & Engineering* **11** 430–444